ELSEVIER

Chemical Geology 191 (2002) 105–119

CHEMICAL GEOLOGY
INCLUDING
ISOTOPE GEOSCIENCE

www.elsevier.com/locate/chemgeo

Trace-element incorporation in titanite: constraints from experimentally determined solid/liquid partition coefficients

M. Tiepolo [a,*], R. Oberti [a], R. Vannucci [a,b]

[a] *CNR-Istituto di Geoscienze e Georisorse, Sezione di Pavia, via Ferrata 1, 27100 Pavia, Italy*
[b] *Dipartimento di Scienze della Terra, Università di Pavia, via Ferrata 1, 27100 Pavia, Italy*

Abstract

Titanite/liquid partition coefficients for most of the trace elements relevant in petrogenetic studies are provided for titanite-saturated liquids equilibrated at 1.5 GPa and 850 °C starting from lamproitic compositions. The high compatibility observed for REE, HFSE, Sr, V and Sc, and the strong incompatibility observed for actinides, large ion lithophile and light elements are discussed in terms of available crystal-chemical mechanisms for incorporation and crystal-structure control.

The exchange vectors Na_1Ca_{-1} and Al_1Ti_{-1} allow local charge balance to be achieved after incorporation of REE^{3+} and R^{5+} at the Ca and Ti site, respectively. The significant amounts of H measured are also relevant in this regard [the exchange mechanism being $(OH)_1O_{-1}$ at the O1 site]. The incorporation of U^{4+} and Th^{4+} at the Ca site is scarce, and is likely balanced by that of Mg^{2+} at the Ti site; both these substitutions are responsible for strong structural strain.

Titanite can thus be considered an important repository for REE and HFSE in metamorphic and igneous rocks, and its role must be accounted for when modelling trace-element residence during metamorphic reactions and late magmatic crystallisation history. Due to the measured differences in compatibility, titanite crystallisation increases the values of Nb/Ta and LREE/HREE ratios in residual liquids. The similar compatibility of U and Pb makes titanite suitable for U–Pb geochronology of igneous rocks only after common Pb correction. Finally, this study confirms that the titanite end member is not suitable for radioactive waste disposal due to the discussed crystal-chemical constraints, and that titanite-based waste forms should contain high amounts of Na^+ and Mg^{2+}.

Keywords: Titanite; Partition coefficients; Trace elements; LA-ICP-MS; Crystal chemistry

1. Introduction

Titanite (general formula $XYOZO_4$, ideally $CaTiOSiO_4$) is a widespread accessory mineral that may contain large amounts of REE and HFSE, and small to moderate amounts of U. It can crystallise both as a primary and as a lower-*T* phase in igneous environments, and also during metamorphic processes involving different bulk compositions (Deer et al., 1982; Nakada, 1991; Gieré, 1992; Franz and Spear, 1985). Thus, titanite is valuable for geochemical modelling of petrogenetic processes. As its closing temperature for the U–Pb isotopic system approaches 600 °C (Cliff et al., 1985; Mezger et al., 1991), titanite can be valuable also for dating high-temperature events.

* Corresponding author. Tel.: +39-382-505882; fax: +39-382-505890.
E-mail address: tiepolo@crystal.unipv.it (M. Tiepolo).

0009-2541/02/$ - see front matter © 2002 Elsevier Science B.V. All rights reserved.
PII: S0009-2541(02)00151-1

The stability field of titanite and the importance of titanite-bearing equilibria have been discussed in several papers (Wones, 1989; Xirouchakis and Lindsley, 1998; Frost et al., 2000; Xirouchakis et al., 2001a,b). For the aim of this work, it is important to recall only that the presence of titanite in igneous rocks is confined to relatively oxidised conditions, whereas reducing conditions favour the formation of titano-magnetite and ilmenite, which are the common Ti-phases in most igneous rocks. Titanite crystallises from intermediate magmas that form diorites and granodiorites, during hydration reactions that convert clinopyroxene to amphibole or oxidation during post-magmatic reequilibration (Frost et al., 2000 and references therein). These considerations suggest that titanite may be only occasionally found in eruptive rocks (Frost and Lindsley, 1991). In metamorphic rocks, titanite may occur in calc-silicate rocks (greenschist to granulite facies) and marbles (greenschist to eclogite grade), in metabasites (upper greenschist and lower amphibolite facies), in low-grade pelitic rocks and in metamorphosed granitic rocks (orthogneisses).

Compounds with the titanite structure are possible candidates as inert phases for nuclear waste disposal (Hayward and Cechetto, 1982; Gascoyne, 1986; Ringwood et al., 1988 and references therein). Titanite also has interesting structural relations with compounds (such as $KTiOPO_4$) with nonlinear optical properties (Kunz et al., 2000 and references therein). Albeit its widespread occurrence in crustal rocks, and its use as a geochronometer (Frost et al., 2000) and as a repository of radionuclides, the incorporation of geochemically relevant elements in titanite is poorly known. Experimentally determined partition coefficients between titanite and melt are available only for a few rare-earth (RE) elements (namely, La, Sm, Ho, Lu; Green and Pearson, 1986), and only for Nb and Ta among high-field-strength (HFS) elements (Green and Pearson, 1987). The major contribution to the understanding of the site preference of minor elements in titanite is that of Perseil and Smith (1995), which is based on a Sb-rich titanite in the manganese concentrations at St. Marcel-Prabona (Italy). The aim of this paper is to provide partition coefficients for an extended set of 25 geochemically relevant elements in the mass range from Li to U measured by both LA-ICP-MS and SIMS techniques, as well as to unravel the crystal-chemical mechanisms controlling trace-element incorporation.

2. Experimental and analytical procedures

2.1. Synthesis

Starting materials (Table 1) used for titanite synthesis were designed to match a silica-rich lamproite from West Kimberley, Australia (Arima and Edgar, 1983). The reason for this choice is that natural lamproites of this composition contain abundant titanite and the addition of sphene components to the starting material is not required. Mg# and Ti contents were also slightly varied from the original lamproite composition in order to control their effects on titanite crystallisation. Starting materials were prepared by properly mixing oxides and carbonates, and the CO_2 component was removed by sintering. Trace elements were added at ppm level as a solid mixture of oxides of LILE, HFSE, REE, light and some transitional elements. Trace-element concentrations and relative proportions were those used by Tiepolo et al. (2000a), and were designed to minimise interference and to optimise counting statistics during LA-ICP-MS analysis.

Experiments were carried out at the University of Göttingen with a single-stage 22-mm piston cylinder apparatus of the type described by Johannes et al. (1971) using polycrystalline CaF_2 assemblies. Details of the experimental procedures are reported in Tiepolo et al. (2000a) Temperature was measured and controlled with $Pt/Pt_{90}Rh_{10}$ thermocouples by a Euro-

Table 1
Nominal major element composition (wt.%) of starting materials

Sample	rb21-1	rb31-3	rb33-3	rb34-3
SiO_2	51.86	51.86	51.86	51.86
TiO_2	11.24	7.88	11.24	11.24
Al_2O_3	2.96	2.96	2.96	2.96
Cr_2O_3	0.10	0.10	0.10	0.10
FeO	7.39	8.90	11.97	14.43
MgO	9.06	10.91	4.48	2.02
CaO	4.21	4.21	4.21	4.21
Na_2O	3.57	3.57	3.57	3.57
K_2O	9.60	9.60	9.60	9.60
Total	100.0	100.0	100.0	100.0

therm 812 controller. Pressures and temperatures were believed to be accurate to ±0.05 GPa and ±15 °C, respectively. Quenching was started by switching off the power supply, and initial quench rates were estimated to be around 80 °C/s.

Experimental charges (18–23 mg) were placed in Pt-capsules (6–8 mm long with a diameter of 4 mm) internally coated with graphite capsules; 15–18 wt.% water was added using a microsyringe. The addition of relatively high H_2O content was required to compensate the loss of water occurring during sealing and annealing, which was shown to exceed 50% by SIMS analysis of H in glasses. The capsules were packed in BN to minimise H loss during the experiments. In this assembly configuration, oxygen fugacity was close to CCO buffer (Tiepolo et al., 2000a). All experiments were pressurised to 0.5 GPa over nominal run pressure and brought to superliquidus conditions (1230 °C) for 1 h. Pressure was then lowered to the run pressure of 1.5 GPa and samples were ramped down to the nominal run temperature of 850 °C at the rate of 1 °C/min, and then kept at the nominal run temperature for 36 h. This procedure ensured complete melting and homogenisation of starting materials, as well as the growth of few homogeneous crystals in all the experiments. After quenching, the capsules were halved with a wire saw, and one part was mounted in epoxy resin and polished for microprobe, LA-ICP-MS and SIMS analyses.

2.2. Analytical techniques

Major elements analyses of titanite and glass were done at the University of Göttingen with a JEOL JXA 8900R electron microprobe operating at 15 kV acceleration voltage and 12 nA beam current. Counting times were 20 s for Cr and Fe, and 16 s for all other major elements. A defocused beam with a diameter of 5 μm was used for all analyses. Mass balance calculations based on modal percentages and Na_2O contents of all the phases in the experimental system (amph, cpx, ttn, and glass) confirmed negligible alkali volatilisation. Mineral standards were wollastonite (Si, Al), albite (Na), sanidine (K) and rutile (Ti); synthetic oxides were used for Cr and Fe.

Trace-element concentrations were measured by LA-ICP-MS at the CNR-Istituto di Geoscienze e Georisorse, Sezione di Pavia (IGG-Pavia). The laser probe used a pulsed Nd:YAG laser source "Brilliant" (Quantel, Les Ulis, France), whose fundamental emission in the infrared (1064 nm) was converted into 266 nm by means of two harmonic generators. For this work, the laser was operated at a repetition rate of 10 Hz, and the spot diameter was 20–40 μm with a pulse energy of about 0.1 mJ. The particles produced by ablation were then analysed by a field-sector mass spectrometer ("Element", Finnigan MAT, Bremen, Germany). Ablation signal integration intervals were selected by carefully inspecting the time-resolved analysis to ensure that no inclusions were present in the analysed volume, and data reduction was done by the software package "Glitter". NIST SRM 610 was

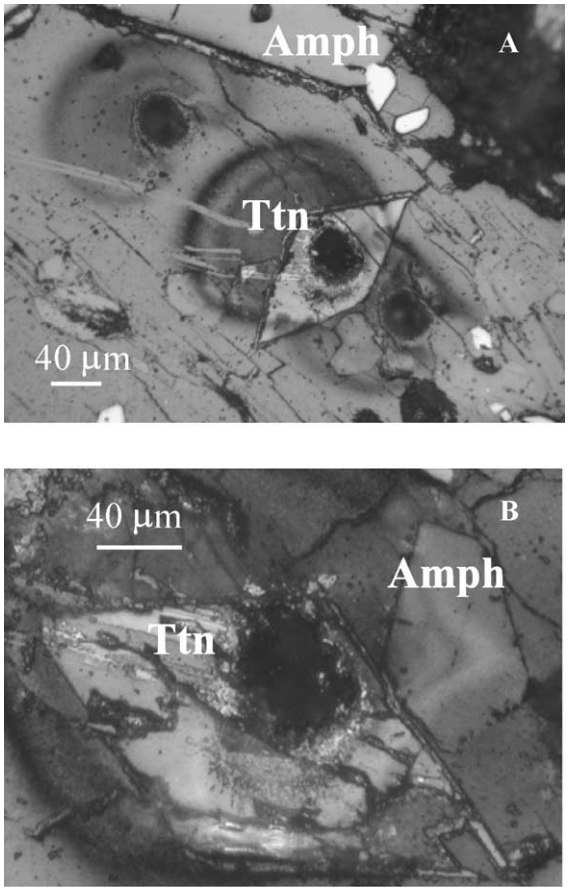

Fig. 1. Microphotographs of the run products. (A) Euhedral titanite dispersed in a quench crystal-free glass. (B) The linear contact between titanite crystals and coexisting amphibole suggests equilibrium conditions among these phases.

Table 2
Major element composition (wt.%) and unit formula (apfu) of titanites

Sample	rb21-1		rb31-3		rb33-3		rb34-3	
Number of analyses	(7)		(5)		(9)		(7)	
SiO_2	28.24	±0.22	28.50	±0.31	29.64	±0.15	29.18	±0.13
TiO_2	40.88	±0.12	39.84	±0.20	39.96	±0.21	39.01	±0.18
Al_2O_3	0.05	±0.01	0.04	±0.01	–	–	0.03	±0.01
Cr_2O_3	0.11	±0.02	–	–	0.15	±0.05	0.54	±0.06
FeO	0.33	±0.03	0.35	±0.04	0.54	±0.02	1.06	±0.10
MgO	0.08	±0.01	0.02	±0.01	–	–	0.06	±0.01
CaO	25.10	±0.14	24.80	±0.12	25.94	±0.20	26.13	±0.16
Na_2O	0.73	±0.04	0.76	±0.03	0.81	±0.04	0.37	±0.01
K_2O	0.01	±0.01	0.07	±0.01	0.10	±0.01	0.10	±0.01
H_2O	0.30	–	0.40	–	–	–	0.15	–
Sc_2O_3	0.22		0.14		0.13		0.14	
SrO	0.02		0.02		0.03		0.01	
Y_2O_3	0.14		0.13		0.13		0.09	
ZrO_2	0.08		0.05		0.04		0.03	
Nb_2O_5	0.07		0.12		0.20		0.08	
La_2O_3	0.10		0.10		0.10		0.04	
Ce_2O_3	0.13		0.13		0.12		0.06	
Nd_2O_3	0.15		0.17		0.15		0.08	
Sm_2O_3	0.37		0.42		0.37		0.20	
Eu_2O_3	0.53		0.60		0.48		0.22	
Gd_2O_3	0.51		0.55		0.49		0.28	
Dy_2O_3	0.76		0.80		0.64		0.42	
Er_2O_3	0.65		0.58		0.38		0.33	
Yb_2O_3	0.75		0.60		0.48		0.37	
HfO_2	0.39		0.29		0.16		0.16	
Ta_2O_5	0.43		0.97		0.95		0.62	
PbO	0.01		0.01		0.02		0.01	
ThO_2	0.08		0.06		0.07		0.07	
UO_2	0.05		0.04		0.04		0.04	
Total	101.29		100.57		102.11		99.86	
Si	0.9602		0.9770		0.9984		0.9913	
Ti	0.0398		0.0230		0.0016		0.0087	
Sum Si site	1.000		1.000		1.000		1.000	
Ti	1.0056		1.0041		1.0108		0.9880	
Al	0.0020		0.0016		0.0000		0.0012	
Fe	0.0046		0.0050		0.0075		0.0149	
Mg	0.0041		0.0010		0.0000		0.0030	
Sc	0.0066		0.0042		0.0037		0.0042	
Nb	0.0011		0.0018		0.0031		0.0013	
Ta	0.0040		0.0091		0.0087		0.0057	
Zr	0.0013		0.0009		0.0007		0.0005	
Hf	0.0038		0.0029		0.0016		0.0016	
Sum Ti site	1.016		1.012		1.018		1.007	
Ca	0.9145		0.9110		0.9363		0.9512	
Na	0.0481		0.0505		0.0529		0.0244	
K	0.0004		0.0031		0.0043		0.0043	
La	0.0013		0.0012		0.0012		0.0005	
Ce	0.0016		0.0017		0.0014		0.0007	
Nd	0.0018		0.0021		0.0018		0.0009	

Table 2 (*continued*)

Sample	rb21-1	rb31-3	rb33-3	rb34-3
Number of analyses	(7)	(5)	(9)	(7)
Sm	0.0044	0.0049	0.0043	0.0024
Eu	0.0062	0.0070	0.0056	0.0025
Gd	0.0057	0.0063	0.0054	0.0031
Dy	0.0084	0.0088	0.0070	0.0046
Y	0.0026	0.0024	0.0024	0.0017
Er	0.0070	0.0062	0.0041	0.0035
Yb	0.0078	0.0063	0.0049	0.0038
Th	0.0006	0.0004	0.0005	0.0005
U	0.0004	0.0003	0.0003	0.0003
Sum Ca site	1.011	1.012	1.032	1.004
OH	0.07	0.09	0.00	0.03
F	0.00	0.00	0.00	0.00
Cl	0.00	0.00	0.00	0.00

used as the external standard, and ^{44}Ca was used as the internal standard.

Light elements (Li, Be and B) and H were determined in both titanite and glass by secondary ion mass spectrometry (SIMS) at the CNR-IGG-Pavia according to the method developed by Ottolini et al. (1993, 1995).

3. Results

3.1. Run products

Run products are amphibole, titanite, subordinate clinopyroxene, rare ilmenite and glass. The degree of crystallisation is lower than 50%, and no quench crystal is present in the glass. Textural relations indicate that amphibole and titanite crystallised at run temperature and not during the downramp from peak *T*. Titanite crystals are strongly euhedral, their size ranging from 50 to 200 μm (Fig. 1A), and do not show significant major-element zoning, as revealed by the low-relative standard deviation in major-element analyses (but for Al, whose content is close to detection limits). Crystal morphology and intragrain homogeneity are good evidences for titanite crystallisation in equilibrium with the surrounding glass. Further evidence is provided by the low standard deviations obtained for major-element contents when averaging random EMP spots in each experimental charge (Table 3). Sharp and linear contacts between titanite and amphibole crystals (Fig. 1B) suggest conditions close to equilibrium also between these mineral phases.

In all the experiments, trace-element contents of the glasses are rather homogenous. Trace-element variations in titanite are within 20% with the only exception of sample rb31-3; they can be regarded as acceptable, possibly suggesting weak zoning. The small crystal size in sample rb31-3 did not allow multiple spots on the same grain; chemical homogeneity is indirectly confirmed by the constancy in all the monitored elements during time-resolved LA-ICP-MS analyses. The differences in REE and HFSE contents measured in this sample, well beyond analytical precision, may reflect either high thermal gradients within the experimental charge or kinetic effects. Nevertheless, the averaged trace element partitioning pattern is consistent with those from the other charges and with the literature, thus precluding selective HFSE uptake by coexisting phases.

Calculation of the titanite unit formula is a very difficult task in the lack of accurate estimates of H, F, REE and also of minor elements, such as transition elements with different possible ionisation states (Oberti et al., 1991; Perseil and Smith, 1995). In the present case, titanite crystallised under controlled physico-chemical conditions, and all the critical elements (including H) were measured by a combination of EMP, SIMS and LA-ICP-MS techniques. The unit formula reported in Table 2 have been obtained based on five oxygen atoms, and considering that the only

not completely controlled variable is the content of monovalent anions at O1 (the accuracy for these low amounts of H is lower than that for other trace elements). All samples are very close in composition and the OH content ranges from 0.03 to 0.09 atoms per formula unit (apfu). The Ti and Ca contents are similar to those observed in magmatic titanites from gabbroic and dioritic rocks (Sondalo and Adamello intrusions; Italian Alps; Fig. 2). Conversely, the Al content is lower (<0.002 apfu) and the Na content is higher (>0.024 apfu). A significant amount (up to 0.040 apfu) of tetrahedral Ti is also observed, which is known to enlarge and distort the tetrahedral site ($^{[4]}$i.r.: 0.26 Å for Si and 0.42 Å for Ti; Shannon, 1976). All these features can be used as indicators of petrogenetic conditions. The lower Ca and Ti contents measured in the synthetic titanites of Green and Pearson (1986, 1987) likely result from the higher contents of Ca substituents (e.g., REE) in the starting materials.

The compositions of the glasses (Table 3) reflect those of the starting materials, so that they can be regarded as analogues of evolved ultrapotassic melts. They are characterised by intermediate SiO_2 contents (55.0 wt.%), high alkali contents (Na_2O+K_2O up to 17.5 wt.%) and low MgO/(MgO+FeO) ratios (0.07–0.3); TiO_2 contents range from 5.0 to 7.4 wt.%. Amphiboles are potassiorichterites according to the nomenclature rules in force (Leake et al., 1997).

Averaged trace-element concentrations in titanite and coexisting glasses are reported in Tables 4 and 5, respectively. Henry's law behaviour was shown for amphiboles crystallised under the same doping level

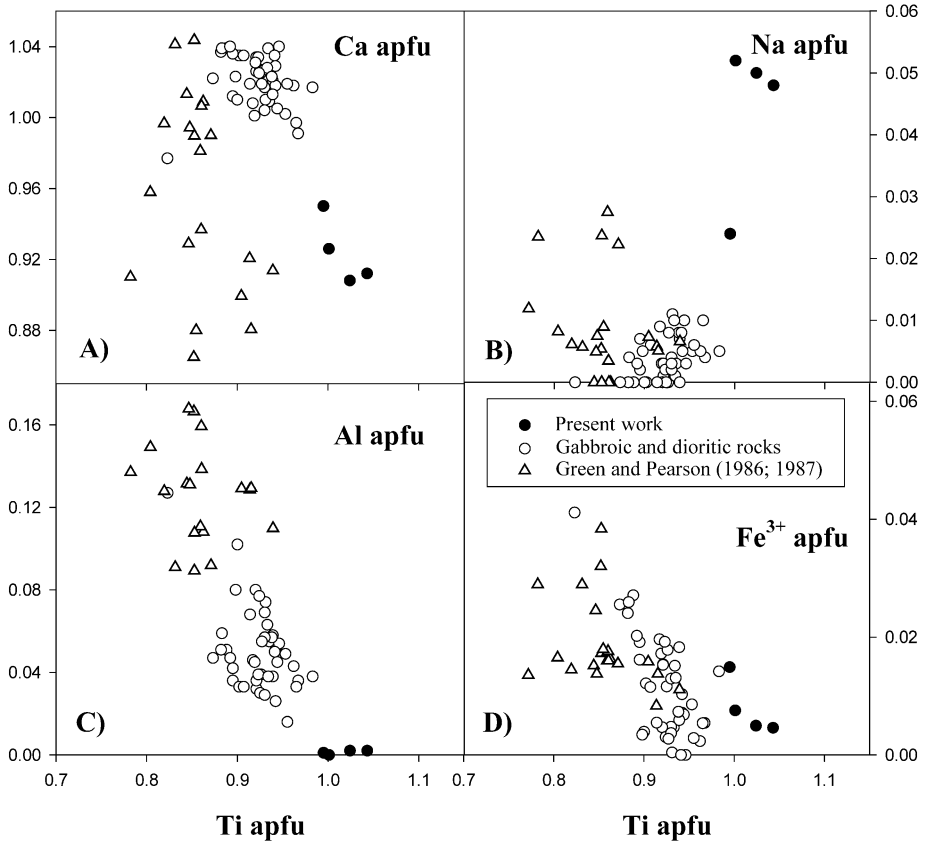

Fig. 2. Variations of the Ti contents vs. the Ca (A), Na (B), Al (C) and Fe^{3+} (D) contents in the synthetic titanites of this work. The synthetic titanites from Green and Pearson (1986, 1987) and some titanites from gabbroic and dioritic rocks from Sondalo and Adamello intrusions are also reported for comparison.

Table 3
Major element composition (wt.%) of glasses coexisting with titanites and 1σ S.D.

Sample	rb21-1		rb31-3		rb33-3		rb34-3	
Number of analyses	(10)		(13)		(15)		(11)	
SiO_2	55.54	±0.19	55.32	±0.08	55.80	±0.82	55.15	±0.29
TiO_2	5.37	±0.07	5.77	±0.03	5.43	±0.06	4.99	±0.08
Al_2O_3	4.57	±0.05	4.87	±0.01	4.29	±0.16	3.86	±0.03
Cr_2O_3	0.02	±0.01	–	–	–	–	0.03	±0.01
FeO	3.03	±0.31	6.44	±0.01	8.49	±0.20	11.09	±0.02
MgO	1.34	±0.26	1.89	±0.01	1.04	±0.01	0.83	±0.01
CaO	2.13	±0.07	0.88	±0.02	0.72	±0.07	0.96	±0.02
Na_2O	1.90	±0.19	2.69	±0.05	4.05	±0.09	4.42	±0.14
K_2O	9.05	±0.26	11.86	±0.27	13.44	±0.09	12.87	±0.09
H_2O	5.20	–	5.90	–	3.80	–	2.00	–
Total	88.15		95.62		97.06		96.20	

in Tiepolo et al. (2000a); it is confirmed by the absence of correlation between $^{Ttn/L}D$ values and concentrations in both titanite and glass observed for the elements with the highest doping level (e.g., Ta, Yb and U).

3.2. Solid/liquid partition coefficients

A minimum of three sets of titanite/melt partition coefficients ($^{Ttn/L}D$) was calculated for each experimental charge from the analyses of adjacent points in

Table 4
Trace element composition (ppm) of synthetic titanites and 1σ S.D.

Sample	rb21-1		rb31-3		rb33-3		rb34-3	
Number of analyses	(4)		(3)		(3)		(3)	
Li	1.41	–	1.37	–	–	–	1.31	–
Be	0.03	–	0.04	–	–	–	0.17	–
B	0.79	–	1.53	–	–	–	1.56	–
Sc	727	±245	462	±99	409	±117	466	±224
V	569	±18	688	±115	237	±66	972	±332
Rb	<6.0	–	<2.8	–	<20	–	<13	–
Sr	188	±21	149	±25	263	±1	83.2	±24
Y	563	±8.0	523	±103	517	±36.5	362	±40.1
Zr	580	±23	396	±197	313	±66	232	±122
Nb	252	±40	416	±221	703	±148	293	±62
Ba	<1.05	–	<0.6	–	<4.0	–	<3.5	–
La	433	±29	413	±191	407	±76	172	±35
Ce	547	±32	573	±217	494	±80	239	±48
Nd	646	±24	732	±228	644	±65	335	±79
Sm	1601	±57	1798	±503	1591	±71	869	±180
Eu	2290	±152	2576	±752	2086	±165	937	±153
Gd	2198	±56	2402	±545	2106	±99	1198	±151
Dy	3321	±28	3470	±822	2802	±46	1813	±144
Er	2856	±94	2518	±544	1681	±174	1430	±137
Yb	3305	±210	2655	±497	2108	±85	1616	±222
Hf	3320	±54	2495	±785	1377	±95	1360	±431
Ta	1764	±100	3987	±1252	3884	±805	2531	±183
Pb	69.7	±12	116	±22	160	±38	74.8	±34
Th	684	±146	506	±279	610	±180	589	±103
U	459	±133	378	±213	340	±70	362	±22

Table 5
Trace element composition (ppm) of glasses and 1σ S.D.

Sample	rb21-1		rb31-3		rb33-3		rb34-3	
Number of analyses	(5)		(4)		(3)		(3)	
Li	117	–	115	–	–	–	127	–
Be	64.3	–	67.5	–	–	–	61.0	–
B	3019	–	2741	–	–	–	1061	–
Sc	301	±22	282	±12	408	±3.7	412	±41
V	105	±7.0	116	±5.2	87.0	±2.3	46.2	±2.6
Rb	1476	±57	1520	±13	1206	±25	1088	±32
Sr	67.9	±4.1	55.8	±0.1	44.8	±0.2	55.4	±1.0
Y	67.3	±4.3	96.5	±0.7	64.3	±3.4	80.1	±1.2
Zr	183	±8.2	206	±2.6	183	±8.1	180	±9.1
Nb	115	±2.8	190	±0.7	146	±4.9	159	±3.7
Ba	339	±17	288	±6.1	259	±2.2	249	±4.4
La	67.4	±4.4	87.4	±1.0	54.3	±1.0	72.0	±0.9
Ce	49.5	±3.6	75.6	±1.5	40.9	±0.4	59.5	±0.5
Nd	34.6	±2.9	59.1	±0.1	27.3	±1.3	44.8	±3.0
Sm	74.9	±7.2	128	±1.6	60.3	±0.2	97.7	±7.0
Eu	112	±8.9	187	±2.9	80.6	±1.8	137	±6.5
Gd	120	±8.7	201	±5.9	104	±7.6	153	±7.8
Dy	270	±23	420	±21	248	±5.5	340	±16
Er	343	±27	454	±23	315	±0.9	391	±39
Yb	732	±42	878	±26	638	±0.2	727	±43
Hf	872	±57	1025	±29	872	±21	877	±65
Ta	234	±17	609	±8.6	440	±20	569	±32
Pb	1268	±134	2612	±35	2173	±48	1615	±393
Th	3120	±205	3137	±15	2242	±106	2400	±461
U	2511	±80	2610	±47	1594	±62	1703	±298

titanite and glass. Table 6 reports the averaged $^{Ttn/L}D$ values for selected elements, as well as their standard deviations.

The corresponding spider diagrams show that most elements (except Li, Be, B, Rb, Ba, U, Th and Pb) are at various extents compatible in titanite (Fig. 3). Light elements, Rb and Ba have the lowest $^{Ttn/L}D$ values (<0.02); given the analytical uncertainty, these should be considered as the maximum values. Pb is strongly incompatible ($^{Ttn/L}D_{Pb}$=0.04–0.07). U and Th are approximately one order of magnitude more compatible than LIL and light elements, and Th is slightly more compatible than U ($^{Ttn/L}D_{U/Th}$=0.78–0.90) in all the experiments. Although the valence of U cannot be directly inferred in our experiments, $^{Ttn/L}D_{U}$ values very close to those of Th suggest that U^{4+} is the dominant species. REE and Y are highly compatible ($^{Ttn/L}D_{REE}$=2.2–26). $^{Ttn/L}D_{REE}$ defines a concave downward pattern with the maximum at Sm (Fig. 3). $^{Ttn/L}D_{La/Sm}$ and $^{Ttn/L}D_{Gd/Yb}$ range from 0.27 to 0.34 and from 3.5 to 6.1, respectively. Ta is the most compatible HFS element ($^{Ttn/L}D$=4.4–8.8), and is strongly fractionated from Nb ($^{Ttn/L}D_{Nb/Ta}$=0.30–0.55). Zr and Hf are less compatible than Nb and Ta ($^{Ttn/L}D_{Zr}$=1.3–3.2), and have nearly the same affinity for titanite ($^{Ttn/L}D_{Zr/Hf}$=0.8–1.0). Partition coefficients for Sr are in the range 1.5–5.8, whereas those for V and Sc range from 2.7 to 21 and from 1.0 to 2.4, respectively.

Comparison with experimentally determined $^{Ttn/L}D$ from literature (Green and Pearson, 1986, 1987) shows that, although the general trend is respected, the $^{Ttn/L}D$ values of this work are lower and characterised by higher LREE/HREE ratios (Fig. 3). The lower D values are likely related to system compositions (i.e., lamproite vs. intermediate-acid silicic melts). Conversely, the different REE fractionation should depend on crystal-chemical constraints, because there is a general consensus that melt does not discriminate among elements with the same

Table 6
Titanite/melt partition coefficients

Sample	rb21-1		rb31-3		rb33-3		rb34-3	
Li	0.01	–	0.01	–	–	–	0.009	–
Be	0.001	–	0.001	–	–	–	0.003	–
B	0.0003	–	0.001	–	–	–	0.011	–
Sc	2.41	±0.83	1.64	±0.36	1.00	±0.29	1.13	±0.56
V	5.43	±0.40	5.94	±1.03	2.72	±0.76	21.0	±7.3
Rb	<0.005	–	–	–	<0.02	–	<0.01	–
Sr	2.77	±0.35	2.68	±0.46	5.88	±0.04	1.50	±0.43
Y	8.36	±0.55	5.42	±1.07	8.04	±0.71	4.52	±0.51
Zr	3.18	±0.19	1.92	±0.96	1.71	±0.37	1.29	±0.68
Nb	2.19	±0.35	2.20	±1.16	4.82	±1.03	1.84	±0.39
Ba	<0.003	–	–	–	<0.02	–	<0.01	–
La	6.43	±0.60	4.73	±2.19	7.50	±1.41	2.39	±0.48
Ce	11.1	±1.04	7.57	±2.88	12.1	±1.95	4.01	±0.81
Nd	18.6	±1.70	12.4	±3.86	23.6	±2.64	7.48	±1.82
Sm	21.4	±2.19	14.0	±3.92	26.4	±1.19	8.89	±1.95
Eu	20.4	±2.10	13.8	±4.02	25.9	±2.13	6.85	±1.17
Gd	18.3	±1.40	11.9	±2.73	20.2	±1.75	7.82	±1.06
Dy	12.3	±1.06	8.27	±2.00	11.3	±0.31	5.33	±0.49
Er	8.32	±0.70	5.54	±1.23	5.34	±0.55	3.66	±0.51
Yb	4.51	±0.39	3.02	±0.57	3.31	±0.13	2.22	±0.33
Hf	3.81	±0.26	2.43	±0.77	1.58	±0.12	1.55	±0.50
Ta	7.54	±0.70	6.55	±2.06	8.82	±1.87	4.44	±0.41
Pb	0.05	±0.01	0.04	±0.01	0.07	±0.02	0.05	±0.02
Th	0.22	±0.05	0.16	±0.09	0.27	±0.08	0.25	±0.06
U	0.18	±0.05	0.14	±0.08	0.21	±0.04	0.21	±0.04

Standard deviations are given at 1σ level.

charge and very similar ionic radii, such as those of the REE group (Watson, 1976; Ryerson and Hess, 1978; Blundy and Wood, 1994).

4. Discussion

4.1. Structure and crystal chemistry of titanite

The $P2_1/a$ titanite structure is generally described in terms of chains of corner-sharing (via O1) octahedra, which run parallel to the crystallographic [100] axis and are cross-linked by isolated tetrahedra (Fig. 4). However, it is relevant to the present discussion that also the [7]-fold-coordinated sites form edge-sharing (via O5 couples) chains which run parallel to [101]. These two chains are also mutually connected by shared edges. Thus, the crystal-chemical mechanisms responsible for electroneutrality at the shared oxygen atoms may involve any combinations of structural sites (e.g., the entrance of $^{Ca}R^{3+}$can be balanced by $^{Ca}R^{1+}$, $^{Ti}R^{3+}$ and $^{Si}R^{3+}$ at the adjacent sites; that of $^{Ca}R^{4+}$ can be balanced by two $^{Ca}R^{1+}$, $^{Ti}R^{2+}$, and two $^{Si}R^{3+}$; etc.).

End member titanite, $CaTiOSiO_4$, is monoclinic, space group $P2_1/a$. In this space group, the octahedral Ti atoms are off-centred, the direction of their shift being coherent along a single octahedral chain and opposite to those occurring in adjacent octahedral chains; this gives rise to antiferroelectric interactions. Phase transitions in titanite as well as in other phases with the titanite structure occur as a function of composition, pressure and/or temperature, and they significantly affect energetic properties. Phase transitions must be taken into account when determining the $P–V–T$ equations of state (Kunz et al., 2000 and references therein), as well as when using a titanite component in energetic modelling. At T>496 K, the ordering in the Ti shifts in $CaTiOSiO_4$ is no longer maintained, and the long-range space group becomes $A2/a$. A $P2_1/a \rightarrow A2/a$ phase transition also occurs in $CaTiOSiO_4$ at high P

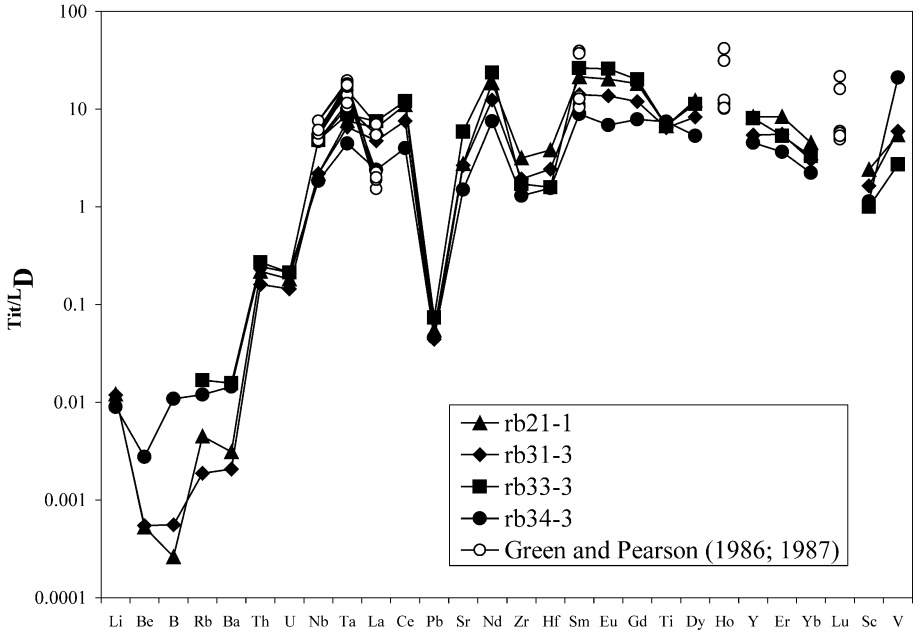

Fig. 3. Spider diagram reporting titanite/melt partition coefficients.

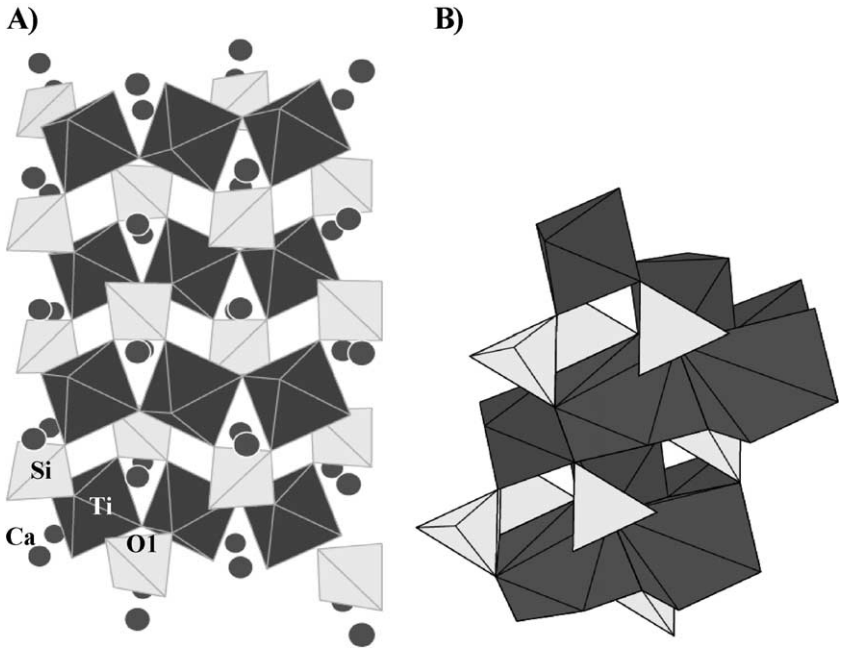

Fig. 4. The structure of titanite. (A) Corner-sharing chains of octahedra parallel to [100]; (B) edge-sharing chains of [7]-fold-coordinated sites running parallel to [101].

(>3.5 GPa), its mechanism is different, and involves the more compressible Ca site, yielding short- and long-range ordering (Kunz et al., 1996; Angel et al., 1999). At T>825 K, a further isosymmetric transition yields a more symmetric Ti coordination (Kek et al., 1997).

In natural titanites, the tetrahedron is fully occupied by Si, whereas the most important chemical species substituting at the octahedral sites are Ti, Al (up to 14 wt.% oxide; Franz and Spear, 1985), Ta (up to 20 wt.% oxide; Cèrny et al., 1995), Sb (up to 11 wt.% oxide; Perseil and Smith, 1995), Nb (up to 5 wt.% oxide; Cèrny et al., 1995) and Fe^{3+} (up to 3 wt.% oxide; Deer et al., 1982). Ca is the dominant species at the [7]-fold-coordinated site, and the presence of Sr and Ba up to 0.009 and 0.006 apfu, respectively, has been reported by Perseil and Smith (1995); REE (up to 0.12 apfu) was shown to enter the Ca site in $^{Ti}R^{3+}$-substituted *A2*/*a* titanites by Huges et al. (1997), the bridging O1 oxygen playing the key role in this couples substitution. In synthetic titanite, some Ti may also occur at the tetrahedral site, with significant effects on tetrahedral and unit-cell dimensions (Oberti et al., 1991). At the octahedral site, complete substitution of Si after Ti at high temperature and pressure has been reported by Angel (1997) and Knoche et al. (1998), and complete Al substitution (paralleled by that of F after O at the O1 bridging oxygen) has been reported at high pressure by Troitzsch et al. (1999). The most important exchange of petrogenetic interest is $Al_1(OH,F)_1Ti_{-1}O_{-1}$, which is related to high-pressure metamorphism. The incorporation of Al at the octahedral site produces a long-range disorder which is expressed by transition to the *A2*/*a* space group (Oberti et al., 1991; Troitzsch and Ellis, 1999; Troitzsch et al., 1999).

4.2. Constraints on trace-element incorporation in titanite

Trace-element incorporation in mineral phases depends on melt composition (Watson, 1976), pressure, temperature (Adam and Green, 1994) and also on the crystal-chemical behaviour of the solid phase. For the latter, the availability of suitable mechanisms to locally balance heterovalent substitutions and the similarity in size of the major and the trace elements are the main ruling criteria. The effect of pressure, temperature and melt composition can be in first approximation neglected for the samples of this work, because P and T have been kept constant in all experiments, and the melts in equilibrium with titanites have nearly the same contents of the elements responsible for polymerisation (e.g., SiO_2 and Al_2O_3). The observed variations in $^{Ttn/L}D$, both in terms of absolute values and of fractionation between the different elements, should thus be related to crystal-chemical variations, and be used to understand the mechanisms controlling trace-element incorporation.

REE^{3+} and $HFSE^{5+}$ (Nb and Ta) have ionic radii similar to those of the major constituent of the [7]-fold-coordinated Ca site and of the octahedral Ti site, respectively. However, they all have one more positive charge. Green and Pearson (1986) investigated the incorporation of some REE in titanite, and concluded that the charge balance mechanism is $^{Ti}[(Al,Fe)_1{}^{3+}Ti_{-1}{}^{4+}]$. Our data show a positive correlation between the calculated strain-compensated partition coefficients for R^{3+} ($D_0{}^{3+}$, cf. Blundy and Wood, 1994; Ca-site parameters in Table 7) and the Al content (Fig. 5A). A positive correlation may also be inferred between the Al content and $^{Ttn/L}D_{Ta}$ (Fig. 5C), albeit the large variation of the former; this evidence suggests that the entrance of Al in adjacent Ti sites locally balances Nb and Ta incorporation at Ti, i.e., $^{Ti}(Ta_1^{5+}Al_1^{3+}Ti_{-2}^{4+})$. Similarly, positive correlations between the Na content and the $^{Ttn/L}D_{REE}$ and $^{Ttn/L}D_{HFSE}{}^{5+}$ values (Fig. 5B and D) demonstrate that the exchange $Na_1^{1+}Ca_{-1}^{2+}$ at adjacent edge-sharing Ca sites enhances REE incorporation at the Ca site in titanite. Huges et al. (1997), who discussed the couples substitution $^{Ti}(Al,Fe)_1^{3+}{}^{Ca}REE_1^{3+}{}^{Ti}Ti_{-1}^{4+}{}^{Ca}Ca_{-1}^{2+}$, had solicited proper experimental work to verify this hypothesis, which is now confirmed by the present work.

The presence of Al^{3+} at the octahedral site decreases its mean bond length ($^{[6]}$i.r., 0.535 Å for

Table 7
Ca-site parameters for R^{3+} calculated with the Blundy and Wood (1994) model

Sample	rb21-1	rb31-3	rb33-3	rb34-3
E (kbar)	4678	4504	6354	4785
r_0 (Å)	1.017	1.018	1.022	1.013
D_0	20.19	13.29	24.56	8.38

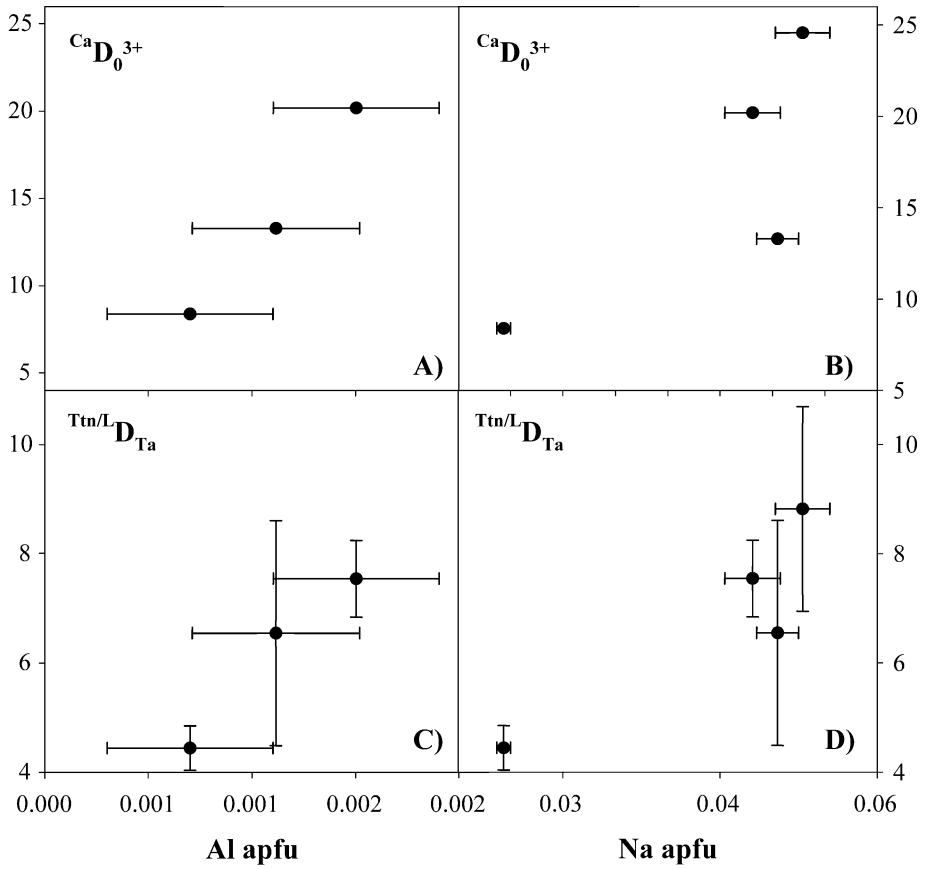

Fig. 5. Variations of the Al content (apfu) vs. $^{VII}D_0^{3+}$ (A) and $^{Ttn/L}D_{Ta}$ (C) and of the Na content (apfu) vs. $^{VII}D_0^{3+}$ (B) and $^{Ttn/L}D_{Ta}$ (D).

Al vs. 0.605 Å for Ti), and favours incorporation of smaller cations. Tiepolo et al. (2000b) on the basis of the behaviour of $^{Amph/L}D$ inferred that ionic radius of Nb is larger than that of Ta; the negative correlation between $^{Ttn}D_{Nb/Ta}$ and Al shown in Fig. 6A is a further confirmation of that statement. At the Ca site, the incorporation of the larger Na cation increases site dimensions, and thus should favour LREE vs. HREE incorporation. Accordingly, Fig. 6B shows a positive relation between the Na content and $^{Ttn/L}D_{La/Yb}$.

The observed incompatibility of Th and U for the titanite structure is mainly related to the difficulty in balancing the two further positive charges. The simultaneous incorporation of Mg^{2+} into an adjacent edge-sharing octahedral site is likely to be the most suitable mechanism. The Mg contents in the samples of this work are very close to the detection limit of the electron microprobe; however, the highest compatibility of U and Th is observed in the titanite sample with the highest Mg contents. Mg is far larger than Ti ($^{[6]}$i.r. 0.72 vs. 0.605 Å), and thus high Mg contents in titanite are unlikely to be hosted in titanite structure. Of the other possible oxidation states, U^{5+} is expected to be even more incompatible (cf. charge-balance), whereas U^{3+} should be compatible in titanite (cf. charge balance and ionic radii).

Sr and Pb are homovalent with Ca, but have larger ionic radii (1.21 and 1.23 Å, respectively, vs. 1.06 Å). Nevertheless, Sr is compatible whereas Pb is incompatible, and their partition coefficients differ by more than one order of magnitude. However, Pb^{2+} has a different electronic configuration, and the presence of stereoactive lone pairs requires a strongly asymmetric coordination, as observed for instance in the amphibole joesmithite.

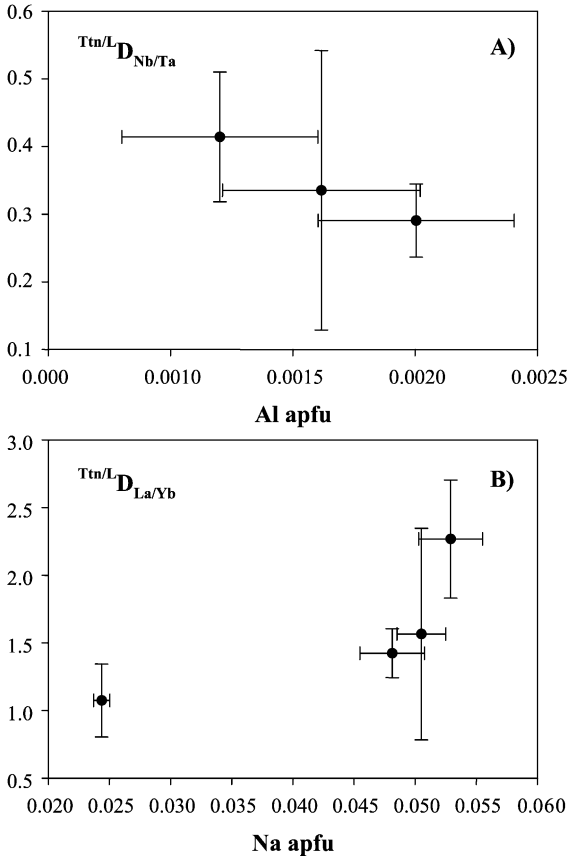

Fig. 6. Variations of the Al content vs. $^{Ttn/L}D_{Nb/Ta}$ (A) and of Na content vs. $^{Ttn/L}D_{La/Yb}$ (B).

The strong incompatibility of Ba and Rb is explained by the lack of structural sites with suitable coordination and size. Detectable Ba contents (0.44 wt.%, corresponding to 0.006 apfu) were observed only by Perseil and Smith (1995) in a Sb-rich titanite crystallised from a very peculiar chemical environment. Both Sc^{3+} and V^{3+} are easily hosted in the octahedral site due to their charge and their ionic radii (0.745 and 0.64 Å, respectively). These latter also explain the lower compatibility observed for Sc than for V.

4.3. Implications for petrogenetic modelling and mineral engineering

This work provides insights into the interpretation of geologic systems where titanite occurs as an accessory phase, and also into mineral engineering aimed to design inert phases for radioactive-waste disposal. Actually, the titanite structure is among the waste forms considered in the SYNROC project (Ringwood et al., 1988 and references therein).

The use of the set of $^{Ttn/L}D$ discussed in the present work is straightforward in lamproitic systems similar to those used as starting material. They can also be applied to other systems in which titanite has a similar crystal chemistry, especially concerning the Na and Al contents which were shown to affect $^{S/L}D$ ratios. In the case of intermediate-acid silicic melts, an error will be most likely introduced. It cannot be estimated directly, but a comparison with $^{Ttn/L}D$ values from Green and Pearson (1986) suggests that it should not exceed a few percent. The solid/liquid partition coefficients presented in this work show that titanite may act as a major repository for many trace elements in many intermediate-acid intrusive rocks such as diorites, where it is often texturally associated with low-Ti green amphibole and plagioclase. During fractional crystallisation processes, low amounts of titanite may significantly increase the Nb/Ta and LREE/MREE ratios in residual liquids. Under the hypothesis of a simple Rayleigh fractional crystallisation process driven only by titanite, 10% crystallisation would multiply by 2 and 5, respectively, the values of the Nb/Ta and La/Sm ratios in the residual melt. They would increase by more than one order of magnitude after less than 30% fractional crystallisation.

The new data provided for U, Th and Pb have important implications for the use of titanite either as a geochronometer or as a repository of toxic and radioactive elements. Given the small difference between their partition coefficients, titanite crystallised from liquids with similar U and Pb contents should be unsuitable for U–Pb geochronology in the absence of an accurate correction for common Pb. On the contrary, the high U concentration observed in titanites from magmatic and metamorphic environments should be ascribed to the circulation of U-rich fluids with high U/Pb values. As suggested by Frost et al. (2000), the required correction for common Pb is minimal in these cases. Concerning the use of titanite for toxic and radioactive waste disposal, crystal-chemical mechanisms controlling elemental incorporation confirm that this structure can be a good repository for HFSE, and suggest that Na- or Al-rich compositions

should be designed for this purpose. On the contrary, titanite is almost of no use for the incorporation of Pb isotopes. Titanite is also expected to be a good repository for Th and U when the starting material is tailored to have significant Mg and very low Na contents at the Ti and Ca sites, respectively.

Acknowledgements

We thank T.H. Green, J. Ayers and D. Xirouchakis for constructive comments, which significantly improved the manuscript. A special thanks to S. Foley and R. Brumm for their help in the experimental procedures and EMP analyses. This research was funded by Ministero dell'Università e della Ricerca Scientifica and Consiglio Nazionale delle Ricerche to CNR-CSCC. **[EO]**

References

Adam, J., Green, T.H., 1994. The effect of pressure and temperature on the partitioning of Ti, Sr, and REE between amphibole, clinopyroxene and basanitic melts. Chem. Geol. 117, 219–233.

Angel, R.J., 1997. Transformation of fivefold-coordinated silicon to octahedral silicon in calcium silicate, $CaSi_2O_5$. Am. Mineral. 82, 836–839.

Angel, R.J., Kunz, M., Miletich, R., Woodland, A.B., Koch, M., Xirouchakis, D., 1999. High-pressure phase transition in $CaTiOSiO_4$ titanite. Phase Transit. 68, 533–543.

Arima, M., Edgar, A.D., 1983. High pressure experimental studies on a katungite and their bearing on the genesis of some potassium-rich magmas of the west branch of the African Rift. J. Petrol. 24, 166–187.

Blundy, J.D., Wood, B., 1994. Prediction of crystal-melt partition coefficients from elastic moduli. Nature 372, 452–454.

Cèrny, P., Novak, M., Chapman, R., 1995. The Al(Nb,Ta)Ti-2 substitution in titanite: the emergence of a new species? Mineral. Petrol. 52, 61–73.

Cliff, R.A., Droop, G.T.R., Rex, D.C., 1985. Alpine metamorphism in the southeast Tauern Window, Austria: II. Heating, cooling and uplift rates. J. Metamorph. Geol. 3, 403–415.

Deer, W.A., Howie, R.A., Zussman, J., 1982. Rock-Forming Minerals. Orthosilicates, vol. 1A. Longman, London.

Franz, G., Spear, F.S., 1985. Aluminous titanite (sphene) from the eclogite zone, South Central Tauern Window, Austria. Chem. Geol. 50, 33–46.

Frost, B.R., Lindsley, D.H., 1991. Occurrence of iron–titanium oxide minerals in igneous rocks. Rev. Miner. 25, 433–486.

Frost, B.R., Chamberlain, K.R., Schumacher, J.C., 2000. Sphene (titanite): phase relations and role as a geochronometer. Chem. Geol. 172, 131–145.

Gascoyne, M., 1986. Evidence for the stability of the potential nuclear waste host, sphene, over geological time, from uranium–lead ages and uranium series measurements. Appl. Geochem. 1, 199–210.

Gieré, R., 1992. Compositional variation of metasomatic titanite from Adamello (Italy). Swiss Bull. Mineral. Petrol. 72, 167–177.

Green, T.H., Pearson, N.J., 1986. Rare-earth element partitioning between sphene and coexisting silicate liquid at high pressure and temperature. Chem. Geol. 55, 105–119.

Green, T.H., Pearson, N.J., 1987. An experimental study of Nb and Ta partitioning between Ti-rich minerals and silicate liquids at high pressure and temperature. Geochim. Cosmochim. Acta 51, 55–62.

Hayward, P., Cechetto, E., 1982. Development of sphene-based glass ceramics tailored for Canadian waste disposal conditions. Topp, S. (Ed.), Scientific Basis for Nuclear Management, vol. 3. Elsevier, Boston, pp. 91–98.

Huges, J.M., Bloodaxe, E.S., Hanchar, J.M., Foord, E.E., 1997. Incorporation of rare earth elements in titanite: stabilization of the *A2*/*a* dimorph by creation of antiphase boundaries. Am. Mineral. 82, 512–516.

Johannes, W., Chipman, D.W., Hays, J.F., Bell, P.M., Mao, H.K., Newton, R.C., Boettcher, A.L., Seifert, F., 1971. An interlaboratory comparison of piston-cylinder pressure calibration using the albite-breakdown reaction. Contrib. Mineral. Petrol. 32, 24–38.

Kek, S., Aroyo, M., Bismayer, U., Schmidt, C., Eichhorn, K., Krane, H.G., 1997. The two-step phase transition of titanite, $CaTiSiO_5$. A synchrotron radiation study. Z. Kristallogr. 212, 9–19.

Knoche, R.L., Angel, R.J., Seifert, F., Fliervoet, T.F., 1998. Complete substitution of Si for Ti in titanite $Ca(Ti_{1-x}Si_x)^{VI}Si^{IV}O_5$. Am. Mineral. 83, 1168–1175.

Kunz, M., Xirouchakis, D., Lindsley, D.H., Häusernann, D., 1996. High-pressure phase transition in titanite ($CaTiOSiO_4$). Am. Mineral. 81, 1527–1530.

Kunz, M., Arlt, T., Stolz, J., 2000. In situ powder diffraction study of titanite ($CaTiOSiO_4$) at high pressure and high temperature. Am. Mineral. 85, 1465–1473.

Leake, B.E., Maresch, W.V., Nickel, E.H., Rock, N.M.S., Schumacher, J.C., Smith, D.C., Stephenson, N.C.N., Ungaretti, L., Whittaker, E.J.W., Youzhi, G., 1997. Nomenclature of amphiboles: report of the subcommittee on amphiboles of the International Mineralogical Association Commission on new minerals and mineral names. Am. Mineral. 82, 1019–1037.

Mezger, K., Rawnsley, S.R., Bohlen, S.R., Hanson, G.N., 1991. U–Pb carnet, titanite, monazite and rutile ages: implications for the duration of high grade metamorphism and cooling histories. J. Geol. 99, 415–428.

Nakada, S., 1991. Magmatic processes in titanite-bearing dacites, central Andes of Chile and Bolivia. Am. Mineral. 76, 548–560.

Oberti, R., Smith, D.C., Rossi, G., Caucia, F., 1991. The crystal-chemistry of high-aluminium titanites. Eur. J. Mineral. 3, 777–792.

Ottolini, L., Bottazzi, P., Vannucci, R., 1993. Quantification of lithium, beryllium, and boron in silicates by secondary ion mass spectrometry using conventional energy filtering. Anal. Chem. 65, 1960–1968.

Ottolini, L., Bottazzi, P., Zanetti, A., Vannucci, R., 1995. Determination of hydrogen in silicates by secondary ion mass spectrometry. Analyst 120, 1309–1313.

Perseil, E.A., Smith, D., 1995. Sb-rich titanite in the manganese concentrations at St. Marcel-Praborna, Aosta Valley, Italy: petrography and crystal-chemistry. Min. Mag. 59, 717–734.

Ringwood, A.E., Kesson, S.E., Reeve, K.D., Levins, D.M., Ramm, E.J. 1988. SYNROC. In: Lutze, W., Ewing, R.C. (Eds.), Radioactive Waste Forms for the Future. North-Holland, Amsterdam, pp. 233–334.

Ryerson, F.J., Hess, P.C., 1978. Implications of liquid–liquid distribution coefficients to mineral–liquid partitioning. Geochim. Cosmochim. Acta 42, 921–932.

Shannon, R.D., 1976. Revised effective ionic radii and systematic studies of interatomic distances in halides and chalcogenides. Acta Crystallogr. 32A, 751–767.

Tiepolo, M., Vannucci, R., Bottazzi, P., Oberti, R., Zanetti, A., Foley, S., 2000a. Partitioning of REE, Y, Th, U and Pb between pargasite, kaersutite and basanite to trachyte melts: implications for percolated and veined mantle. Geochem. Geophys. Geosyst. 1. Paper number 2000GC000064 [9150 words, 11 figures, 3 tables, 4 appendix tables].

Tiepolo, M., Vannucci, R., Oberti, R., Foley, S., Bottazzi, P., Zanetti, A., 2000b. Nb and Ta incorporation and fractionation in titanian pargasite and kaersutite: crystal-chemical constraints and implications for natural systems. Earth Planet. Sci. Lett. 176, 185–200.

Troitzsch, U., Ellis, D.J., 1999. The synthesis and crystal structure of $CaAlFSiO_4$, the Al-F analog of titanite. Am. Mineral. 84, 1162–1169.

Troitzsch, U., Ellis, D.J., Thompson, J., Fitz-Gerald, J., 1999. Crystal structural changes in titanite along the join TiO–AlF. Eur. J. Mineral. 6, 955–965.

Watson, E.B., 1976. Two-liquid partition coefficients: experimental data and geochemical implications. Contrib. Mineral. Petrol. 56, 119–134.

Wones, D., 1989. Significance of the assemblage titanite+magnetite+quartz in granitic rocks. Am. Mineral. 74, 744–749.

Xirouchakis, D., Lindsley, D.H., 1998. Equilibria among titanite, hedenbergite, fayalite, quartz, ilmenite, and magnetite: experiments and internally consistent thermodynamic data for titanite. Am. Mineral. 83, 712–725.

Xirouchakis, D., Lindsley, D.H., Andersen, D.J., 2001a. Assemblages with titanite (CaTiOSiO4), Ca–Mg–Fe olivine and pyroxenes, Fe–Mg–Ti oxides, and quartz: Part I. Theory. Am. Mineral. 86, 247–253.

Xirouchakis, D., Lindsley, D.H., Andersen, D.J., 2001b. Assemblages with titanite (CaTiOSiO4), Ca–Mg–Fe olivine and pyroxenes, Fe–Mg–Ti oxides, and quartz: Part II. Application. Am. Mineral. 86, 254–264.